AIAA JOURNAL
Vol. 43, No. 8, August 2005

Perturbed Compressible Equations for Aeroacoustic Noise Prediction at Low Mach Numbers

Jung-Hee Seo* and Young J. Moon†
Korea University, Seoul 136-701, Republic of Korea

A revised formulation of a hydrodynamic/acoustic splitting method is proposed for aeroacoustic noise prediction of wall-bounded shear flows at low Mach numbers. Based on the analysis of perturbed vorticity transport equation, a set of perturbed compressible equations (PCE) is derived to handle properly the near-field compressibility effects. The accuracy of the formulation is verified for a dipole tone of laminar flow past a circular cylinder at freestream Mach number $M_\infty = 0.3$ and Reynolds number based on the cylinder diameter, $Re_D = 200$. It is shown that the computational results of PCE are in excellent agreement with those of direct acoustic numerical simulation (DNS) and Curle's acoustic analogy. Finally, the computational efficiency of the present PCE is demonstrated by employing an acoustic grid coarser than the hydrodynamic grid such that a time step can be shared for both. It is found that PCE is about three times faster than DNS for the present cylinder tone problem and this speed-up can be increased up to 5–7 for Mach numbers less than 0.2.

I. Introduction

In recent years, aeroacoustic noise prediction has progressed via direct numerical simulation (DNS) of the compressible Navier–Stokes equations. Because the generation and propagation of acoustic waves are sought as a part of the solution in addition to the hydrodynamic field, DNS can provide the physics of aeroacoustics in detail. The DNS for low Mach number flows, for example, $M < 0.3$, however, remains a difficult and challenging problem because a scale disparity between the speed of sound and the material velocity restricts the time step severely.

To resolve the issue of scale disparity, a viscous/acoustic splitting method has been proposed by Hardin and Pope.[1,2] This method splits the DNS into the viscous/hydrodynamic and inviscid/acoustic calculations. The viscous flowfield is computed by solving the incompressible Navier–Stokes equations, whereas the acoustic field is obtained by the perturbed Euler equations (PEE). This splitting method has further been modified by Shen and Sorenson[3–5] and Slimon et al.[6,7] These methods have been quantitatively verified for a quadruple noise generated by a spinning vortex pair[6–8] in an unbounded flow domain, but none of these methods[3–6] have been critically validated for the dipole noise from a wall-bounded shear flow. Shen and Sorenson[3,4] tested their formulation for a dipole tone generated by vortex shedding from a circular cylinder at $M_\infty = 0.2$ and 0.3 and $Re_D = 200$, but the computed results have not been verified with experimental data or analytical solution. Actually, their solution shows some numerical errors[4] caused by a fundamental deficiency of the previous viscous/acoustic splitting methods.[1–7] The same dipole tone problem was also tested by Slimon et al.[6] for $M_\infty = 0.2$ and $Re_D = 9 \times 10^4$ and compared with the experimental data. The selected Reynolds number is, however, in the subcritical regime ($10^3 < Re_D < 2 \times 10^5$), where the laminar boundary layer on the cylinder immediately transits to turbulence and the wake is fully three dimensional. A two-dimensional Reynolds averaged Navier–Stokes calculation by Slimon et al.[6] cannot be considered proper in the first place.

The perturbed quantities in the viscous/acoustic splitting method are essentially the differences between the compressible and incompressible flowfields, mainly caused by compressibility effects. The perturbed quantities can be regarded as acoustic fluctuations at the far field,[1–7] but for noise from a wall-bounded shear flow, these may represent more complicated features in the near field, for example, a coupling effect between the incompressible vorticity and the perturbed velocities. This coupling effect can be manifested significantly in the vicinity of the wall, and so it should carefully be handled in the splitting method, although it has not been given much attention in previous studies.[1–8]

For this reason, a revised formulation of hydrodynamic/acoustic splitting method is proposed in the present study. A set of perturbed compressible equations (PCE) is derived to handle the near-field compressibility (or coupling) effect properly. In the revised formulation, the perturbed viscous stresses are included in the momentum equations to handle the viscous diffusion of the perturbed vorticity near the wall, and a new perturbed energy equation is derived in a more formal way. In this study, the present PCE is validated for a dipole tone of laminar flow past a circular cylinder at a freestream Mach number $M_\infty = 0.3$ and Reynolds number based on cylinder diameter, $Re_D = 200$, by comparing it with the DNS and Curle's acoustic analogy solutions.

In Sec. II, a DNS solution is presented for the cylinder laminar tone at $M_\infty = 0.3$ and $Re_D = 200$. Then, the PCE is derived in Sec. III, with an analysis of the source terms in the perturbed vorticity transport equation. A high-order numerical scheme and the boundary conditions are described in Sec. IV. In Sec. V, the PCE is validated with the DNS and Curle's acoustic analogy solutions, followed by a discussion on possible error sources in the PEE, and finally a computational efficiency of the PCE is demonstrated, using different grids for the incompressible viscous flow and the acoustic field, respectively.

II. DNS

Laminar flow past a circular cylinder at $M_\infty = 0.3$ and $Re_D = 200$ is considered for validation of the present PCE. To obtain a faithful solution to this problem, a DNS is carried out by solving the full compressible Navier–Stokes equations, with flow variables nondimensionalized by speed of sound a_∞, cylinder diameter D, density ρ_∞, pressure $\rho_\infty a_\infty^2$, and temperature T_∞. The governing equations are spatially discretized by a sixth-order compact finite difference scheme[9] and integrated in time using a four-stage Runge–Kutta method. Numerical details are described in Sec. IV.

Presented as Paper 2003-3270 at the AIAA/CEAS 9th Aeroacoustics Conference, Hilton Head, SC, 12–14 May 2003; received 10 February 2004; revision received 1 March 2005; accepted for publication 28 March 2005.

*Ph.D. Candidate, Department of Mechanical Engineering. Student Member AIAA.

†Professor, Department of Mechanical Engineering; yjmoon@korea.ac.kr. Senior Member AIAA.

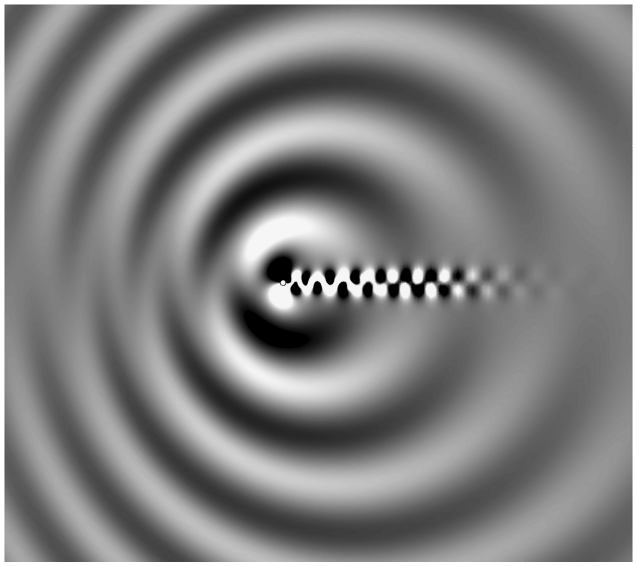

Fig. 1 Instantaneous pressure fluctuation $\Delta p'(=p-\bar{p})$ field around a circular cylinder (DNS, $M_\infty = 0.3$, $Re_D = 200$, and $-50D < x, y < 50D$).

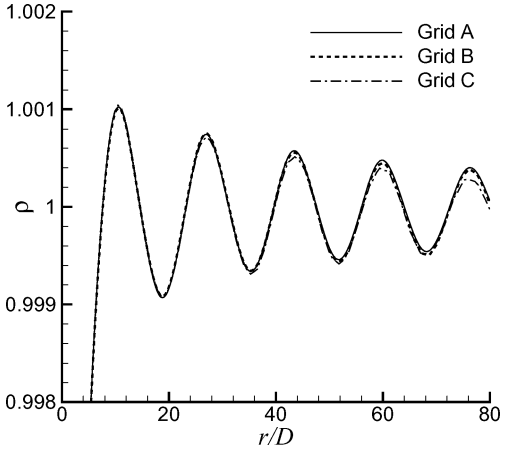

Fig. 2 Instantaneous density variation along $\theta = 90$ deg line (grid A, 401 × 601; grid B, 201 × 201; and grid C, 141 × 151).

A computational domain is set to $r = 100D$ and an O-type grid is used with 201 × 201 mesh points. An instantaneous pressure fluctuation field $\Delta p'(= p - \bar{p})$ is presented in Fig. 1, where one can clearly see the dipole acoustic wave radiation and the von Kármán vortex street in the domain, $-50D < x, y < 50D$. A grid-dependency study is also performed with three different grids: grid A (401 × 601), grid B (201 × 201), and grid C (141 × 151). The test results are compared in Fig. 2, which shows the instantaneous density variation along the $x = 0$ line above the cylinder. Notice that grids A and B are almost identical, but some discrepancy is observed for grid C. Therefore, grid B (201 × 201) is chosen for all other computations.

In this study, the DNS solution is validated by comparing with the two-dimensional Curle's acoustic analogy solution, obtained with the surface pressure fluctuation data extracted from the DNS solution. When only the dipole noise is considered, the modified Curle's solution (see Ref. 10) is written as

$$\Delta p'_{\text{Curle}}(\boldsymbol{x}, t) = \frac{1}{2^{\frac{3}{2}}\pi c_\theta^{\frac{1}{2}} r'^{\frac{1}{2}}} \int_{-\infty}^{\tau} \frac{1}{\sqrt{\tau - \tau'}} \frac{\partial}{\partial \tau'} \left[\frac{x'_i}{r'} F_i(\tau') \right] \mathrm{d}\tau' \quad (1)$$

where $r' = |x'|$. $\tau = t - r'/c_\theta$, F_i are lift and drag forces, and $c_\theta = c_\infty[\sqrt{(1 - M_\infty^2 \sin^2\theta)} - M_\infty \cos\theta]$ is a correction factor to take into account the Doppler effect. Figure 3 shows that a directivity of the instantaneous pressure fluctuation (root mean squared), $\Delta p'_{\text{rms}}$ at $r = 60D$, is very close when compared with that of the Curle's

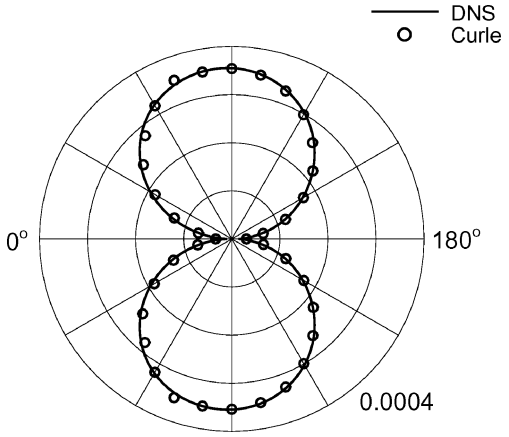

Fig. 3 Directivity of pressure fluctuation (rms), $\Delta p'_{\text{rms}}$ at $r = 60D$.

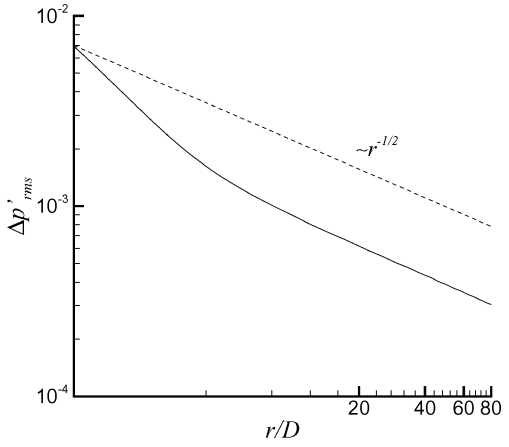

Fig. 4 Pressure fluctuation (rms), $\Delta p'_{\text{rms}}$ variation along $\theta = 90$ deg line.

acoustic analogy. Figure 4 shows the variation of $\Delta p'_{\text{rms}}$ along the $\theta = 90$ deg line, indicating that it decays as $\sim r^{-\frac{1}{2}}$ in the far field, that is, $r/D > 10$ for this problem, strictly obeying two-dimensional acoustic wave theory.

III. PCE

In the hydrodynamic/acoustic splitting method, the instantaneous total flow variables are decomposed into incompressible and perturbed compressible varibles as

$$\rho(x, t) = \rho_0 + \rho'(x, t) \quad (2)$$

$$u_i(x, t) = U_i(x, t) + u_i'(x, t) \quad (3)$$

$$p(x, t) = p(x, t) + p'(x, t) \quad (4)$$

The incompressible flow variables describe unsteady viscous flow, whereas the perturbed variables essentially represent the differences between the compressible and incompressible flowfields. These differences are mainly caused by compressibility effects, and the perturbed quantities can be regarded as acoustic fluctuations at the far field (irrotational field, i.e., $\nabla \times \boldsymbol{u}' = 0$). For noise from a wall-bounded shear flow, however, these quantities could represent more complicated features, for example, a coupling effect between the two states. Thus, it should be handled carefully in the splitting method.

This coupling effect has not been much paid attention in the previous studies,[1–7] but its role in the near-field dynamics may be critically important, especially when an acoustic source is in the wall-bounded shear flow. Hence, it is necessary to investigate the dynamics of perturbed vorticity ω' defined as

$$\boldsymbol{\omega}' = \nabla \times \boldsymbol{u}' \quad (5)$$

Because the velocity field is linearly decomposed, the vorticity field in the compressible flow can also be linearly decomposed into the incompressible and perturbed compressible variables:

$$\boldsymbol{\omega}(x,t) = \boldsymbol{\Omega}(x,t) + \boldsymbol{\omega}'(x,t) \tag{6}$$

To derive a transport equation of $\boldsymbol{\omega}'$, the compressible and incompressible vorticity transport equations are considered. The vorticity transport equations are written as

$$\frac{\partial \boldsymbol{\omega}}{\partial t} + (\boldsymbol{u}\cdot\nabla)\boldsymbol{\omega} = -\boldsymbol{\omega}(\nabla\cdot\boldsymbol{u}) + (\boldsymbol{\omega}\cdot\nabla)\boldsymbol{u} + \nabla\times\boldsymbol{F}_{\mathrm{vis},C} - \nabla\times\left(\frac{1}{\rho}\nabla p\right) \tag{7}$$

$$\frac{\partial \boldsymbol{\Omega}}{\partial t} + (\boldsymbol{U}\cdot\nabla)\boldsymbol{\Omega} = (\boldsymbol{\Omega}\cdot\nabla)\boldsymbol{U} + \nabla\times\boldsymbol{F}_{\mathrm{vis},I} \tag{8}$$

where $\boldsymbol{F}_{\mathrm{vis},C}$ and $\boldsymbol{F}_{\mathrm{vis},I}$ are the compressible and incompressible viscous force vectors, respectively. When Eq. (6) is substituted into Eq. (7) and Eq. (8) is subtracted from Eq. (7), a perturbed vorticity transport equation is derived as

$$\frac{\partial(\boldsymbol{\omega}'/\rho)}{\partial t} + (\boldsymbol{u}\cdot\nabla)\left(\frac{\boldsymbol{\omega}'}{\rho}\right) = \frac{1}{\rho}[(\boldsymbol{\Omega}\cdot\nabla)\boldsymbol{u}' + (\boldsymbol{\omega}'\cdot\nabla)\boldsymbol{u}] - \frac{1}{\rho}[(\boldsymbol{u}'\cdot\nabla)\boldsymbol{\Omega} + \boldsymbol{\Omega}(\nabla\cdot\boldsymbol{u}')] + \frac{1}{\rho}\nabla\times\boldsymbol{F}'_{\mathrm{vis}} + \frac{1}{\rho^3}(\nabla\rho\times\nabla p) \tag{9}$$

where $\boldsymbol{F}'_{\mathrm{vis}} = \boldsymbol{F}_{\mathrm{vis},C} - \boldsymbol{F}_{\mathrm{vis},I}$. For a two-dimensional flow, Eq. (9) can be reduced to

$$\frac{\partial(\omega'/\rho)}{\partial t} + (\boldsymbol{u}\cdot\nabla)\left(\frac{\omega'}{\rho}\right) = -\frac{1}{\rho}[(\boldsymbol{u}'\cdot\nabla)\Omega + \Omega(\nabla\cdot\boldsymbol{u}')] + \frac{1}{\rho}\nabla\times\boldsymbol{F}'_{\mathrm{vis}} + \frac{1}{\rho^3}(\nabla\rho\times\nabla p) \tag{10}$$

where ω' and Ω are the surface normal components of the vorticity vectors.

The first three terms on the right-hand side of Eq. (10) are considered important when noise is generated by vortex motions near the wall. These terms will act as a source for production and decay of ω'. The first two terms are related to the coupling effect between the incompressible vorticity field Ω and the perturbed velocity field $\boldsymbol{u}'$. More specifically, the first term, $(\boldsymbol{u}\cdot\nabla)\Omega$, represents the convection of incompressible vorticity Ω by the perturbed velocity $\boldsymbol{u}'$ and the second term, $\Omega(\nabla\cdot\boldsymbol{u}')$, is associated with the effect of dilatation rate. The third term is responsible for the molecular diffusion of ω' by the perturbed viscous force $\boldsymbol{F}'_{\mathrm{vis}}$.

In the previous viscous/acoustic splitting methods,[1–7] the PEE were derived, dropping off the viscous terms. Hence, near the wall where Ω is most intensive, PEE with a slip-wall boundary condition could excessively generate ω' through the coupling effect between Ω and $\boldsymbol{u}'$ by the production term $(\boldsymbol{u}'\cdot\nabla)\Omega$. Moreover, a disregard of viscous diffusion term would not provide any physical diffusion mechanism for ω' in the near field. Therefore, the false behavior of the excessively generated ω' field could seriously affect the acoustic far field. The effect of dilatation rate is, on the other hand, expected to be weak for the present low-Mach-number flow applications. Only a two-dimensional flow case is discussed so far, but one can expect an additional coupling effect from the vortex stretching in the three-dimensional cases. More detailed analysis on this issue will be presented in Sec V.

For the aforementioned reasons, an introduction of perturbed viscous stress τ'_{ij} [which appears as $\boldsymbol{F}'_{\mathrm{vis}}$ in Eq. (10)] will not only properly diffuse the ω' field but also provide a physical basis for using a no-slip boundary condition for u'_i at the wall. The no-slip boundary condition will not generate ω' at the wall by the production term $(\boldsymbol{u}'\cdot\nabla)\Omega$. In addition, a viscous layer of $\boldsymbol{u}'$ will be formed near the wall so that the production of ω' by $(\boldsymbol{u}'\cdot\nabla)\Omega$ would not be as excessive as in the case of PEE. The effect and role of perturbed viscous stresses will also be discussed in Sec V.

Based on the analysis of perturbed vorticity dynamics at the near field, the perturbed continuity and momentum equations are derived as

$$\frac{\partial\rho'}{\partial t} + \frac{\partial}{\partial x_i}(\rho u'_i + \rho' U_i) = 0 \tag{11}$$

$$\frac{\partial(\rho u'_i + \rho' U_i)}{\partial t} + \frac{\partial}{\partial x_j}[u_j(\rho u'_i + \rho' U_i)] + \frac{\partial}{\partial x_j}(\rho_0 U_i u'_j) + \frac{\partial p'}{\partial x_i} = \frac{\partial \tau'_{ij}}{\partial x_j} \tag{12}$$

In the present formulation, the perturbed viscous stresses τ'_{ij} are retained in the perturbed momentum equations, which are defined as differences between the compressible and incompressible viscous stresses. If the viscosity parameter is assumed constant as $\mu \approx \mu_0 = \mu_\infty$ at low Mach numbers, then the perturbed viscous stresses can be simplified to a form similar to the compressible viscous stresses:

$$\tau'_{ij} = \mu_0\left(\frac{\partial u'_i}{\partial x_j} + \frac{\partial u'_j}{\partial x_i} - \frac{2}{3}\frac{\partial u'_k}{\partial x_k}\delta_{ij}\right) \tag{13}$$

To close the PCE, an energy equation is needed for the perturbed properties. Derivation of this equation is not obvious because there is no related incompressible counterpart. Therefore, previous researchers derived it through various modelings or simplifications of the flowfield.[1–6] In the present study, a more general and accurate form is derived with the compressible thermal energy equation. The compressible thermal energy equation is written as

$$\frac{\partial}{\partial t}\left(\frac{p}{\gamma-1}\right) + u_j\frac{\partial}{\partial x_j}\left(\frac{p}{\gamma-1}\right) + \frac{\gamma p}{\gamma-1}\frac{\partial u_j}{\partial x_j} = \phi - \frac{\partial q_j}{\partial x_j} \tag{14}$$

where φ is a viscous dissipation term and q_j is the heat flux. When variable decomposition is applied to Eq. (14), a perturbed energy equation is then derived as

$$\frac{\partial p'}{\partial t} + u_j\frac{\partial p'}{\partial x_j} + \gamma p\frac{\partial u'_j}{\partial x_j} = -\left(\frac{\partial P}{\partial t} + u_j\frac{\partial P}{\partial x_j}\right) + (\gamma-1)\left(\phi - \frac{\partial q_j}{\partial x_j}\right) \tag{15}$$

Because there are no terms neglected or modeled, Eq. (15) can be considered as a general form of the perturbed energy equation for p'. To use Eq. (15), the incompressible pressure field must be rescaled as $P_\infty = \rho_0 a_\infty^2/\gamma$.

Finally, a set of PCE can be expressed in nonconservative form as

$$\frac{\partial\rho'}{\partial t} + u_j\frac{\partial\rho'}{\partial x_j} + \rho\frac{\partial u'_j}{\partial x_j} = 0 \tag{16}$$

$$\frac{\partial u'_i}{\partial t} + u_j\frac{\partial u'_i}{\partial x_j} + \frac{1}{\rho}\frac{\partial p'}{\partial x_i} + u'_j\frac{\partial U_i}{\partial x_j} + \frac{\rho'}{\rho}\frac{\mathrm{D}U}{\mathrm{D}t} = \frac{1}{\rho}\frac{\partial\tau'_{ij}}{\partial x_j} \tag{17}$$

$$\frac{\partial p'}{\partial t} + u_j\frac{\partial p'}{\partial x_j} + \gamma p\frac{\partial u'_j}{\partial x_j} + u'_j\frac{\partial P}{\partial x_j} = -\frac{\mathrm{D}P}{\mathrm{D}t} + (\gamma-1)\left(\phi - \frac{\partial q_j}{\partial x_j}\right) \tag{18}$$

where $\mathrm{D}/\mathrm{D}t = \partial/\partial t + U_j\partial/\partial x_j$.

The incompressible Navier–Stokes equations and the PCE are a two-step splitting approach to the direct simulation of the full compressible Navier–Stokes equations, and the term $\mathrm{D}P/\mathrm{D}t$ on the right-hand side of Eq. (17) is considered as the only explicit connecting chain between the incompressible Navier–Stokes equations and the PCE. Even though the last two terms on the right-hand side of Eq. (18) are retained as a formal expression for the perturbed energy

equation, the effects of these terms are expected to be insignificant in the low-Mach-number flow applications with no thermal effect. Also note that the perturbed quantities are not easy to be comprehended because they represent diverse compressibility effects. Thus, they should be reconstructed into the total flow variables, to have a physical meaning.

IV. Computational Methods

The governing equations are spatially discretized with a sixth-order compact finite difference scheme[9] to avoid excessive numerical dissipations and dispersions errors. A first derivative with respect to x is calculated implicitly with a five point stencil via

$$\alpha f'_{i-1} + f'_i + \alpha f'_{i+1} = a\frac{f_{i+1} - f_{i-1}}{2\Delta x} + b\frac{f_{i+2} - f_{i-2}}{4\Delta x} \qquad (19)$$

where $\alpha = 1/3$, $a = 14/9$, and $b = 1/9$.

The governing equations are transformed into the curvilinear coordinates using a Jacobian transformation, and the metrics are also calculated by the compact scheme to retain the order of accuracy.[11,12] The equations are integrated in time by a four-stage Runge–Kutta method and a 10-order spatial filtering proposed by Gaitonde et al.[13] is applied every iteration to suppress the high-frequency errors that might be caused by grid nonuniformity.

At the far-field boundaries, Freund's buffer zone-type boundary condition[14] is employed to handle the outgoing acoustic waves. At the solid wall, a no-slip boundary condition is used for the incompressible viscous flow calculation ($U = V = 0, \partial P/\partial n = 0$) and also for the DNS and PCE calculations with an adiabatic wall treatment, for example, PCE, $u' = v' = 0$, $\partial p'/\partial n = 0$, and $\partial \rho'/\partial n = 0$. The incompressible Navier–Stokes equations are time accurately solved by a projection-method-based algorithm.[15] The PCE calculation starts with an incompressible flow solution once a periodic stage is developed, and an initial condition of $u'_i = 0$, $p' = 0$, $\rho' = (P - P_\infty)/a^2_\infty$ is used for PCE.

V. Results and Discussion

A. Validation of PCE

A dipole tone of laminar flow past a circular cylinder at $M_\infty = 0.3$ and $Re_D = 200$ is considered for validation of the present PCE. A computational grid (201×201), with which the incompressible Navier–Stokes equations are solved, is also used in the PCE calculation, to exclude any possible interpolation error between the two grid systems for flow and acoustics. For comparison, the acoustic field is also calculated with PEE.[3,4]

The instantaneous pressure fluctuation $\Delta p'$ fields from DNS, PCE, and PEE are presented in Fig. 5. For PCE and PEE, $\Delta p'$ is defined as

$$\Delta p' = (P + p') - \overline{(P + p')} \qquad (20)$$

where the overbar indicates a time-averaged quantity.

The PCE solution is in excellent agreement with the DNS solution, whereas the PEE yields an acoustic field noticeably different from them. In the PEE solution, the computed vortices are very irregular, and the acoustic field is considerably affected by their motions around the cylinder as well as in the downstream wake. The time history of $\Delta p'$ at $r = 60D$ and $\theta = 90$ deg (Fig. 6) also shows that the PEE exhibits quite irregular pressure fluctuations with an unexpected low-frequency component,[4] whereas the PCE solution is in excellent agreement with the DNS solution. Variation of $\Delta p'$ along the $\theta = 90$ deg line and the directivity of $\Delta p'_{\text{rms}}$ at $r = 60D$ are also compared in Fig. 7 between the solutions of DNS, Curle's acoustic analogy, PCE, and PEE. Figure 7 shows that the PCE solution agrees very nicely with the DNS and Curle's acoustic analogy solutions, whereas there is a substantial amount of deviations found in the PEE solution.

Now, it is necessary to investigate why PEE yields such a deviated acoustic solution. Because the cylinder tone strongly depends on the characteristics of vortex shedding, it is conjectured that irregular fluctuations of acoustic pressure in PEE are due to the false

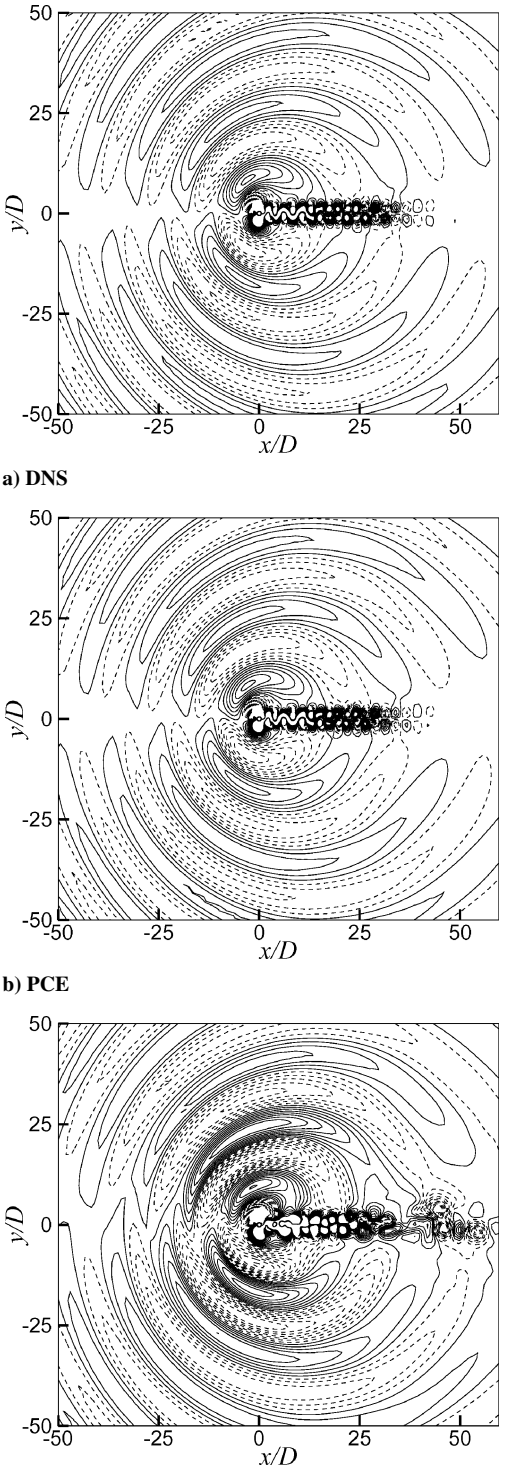

Fig. 5 Instantaneous pressure fluctuation $\Delta p'$ around circular cylinder ($M_\infty = 0.3$, $Re_D = 200$, 20 contours between -0.002 and 0.002).

behavior of excessively generated perturbed vorticity ω' near the cylinder as well as due to the fact that there was no proper diffusion of ω'. Figure 8 shows the contours of perturbed vorticity field and its production terms $(\boldsymbol{u}' \cdot \boldsymbol{\nabla})\Omega$ and $\Omega(\boldsymbol{\nabla} \cdot \boldsymbol{u}')$ for PCE and PEE. Notice that the perturbed vorticity field near the cylinder is mainly generated by the production term $(\boldsymbol{u}' \cdot \boldsymbol{\nabla})\Omega$, that is, convection of incompressible vorticity Ω by perturbed velocity $\boldsymbol{u}'$, whereas the effect of dilatation rate $\Omega(\boldsymbol{\nabla} \cdot \boldsymbol{u}')$ is very small. Because the PEE calculation was conducted with a slip-wall boundary condition, the production of ω' by $(\boldsymbol{u}' \cdot \boldsymbol{\nabla})\Omega$ is most intensive near the wall (Fig. 8b). This will then eventually lead to generation of

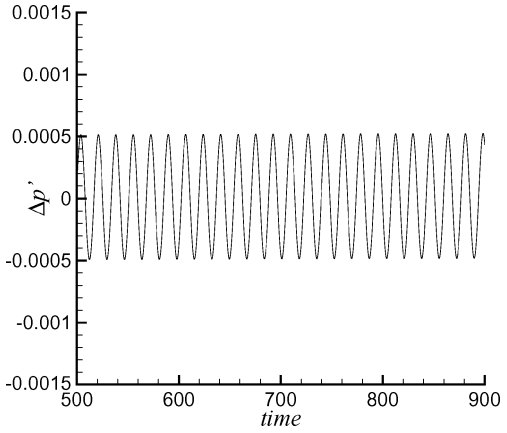

a) DNS

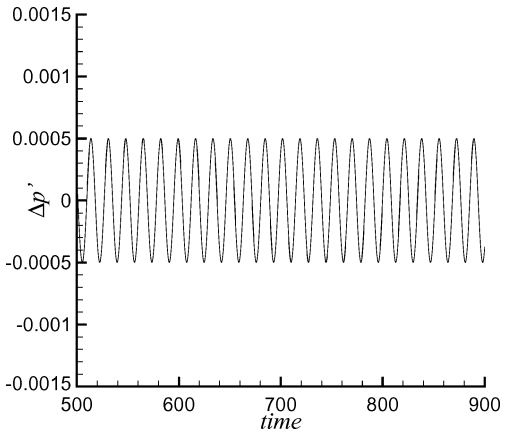

b) PCE

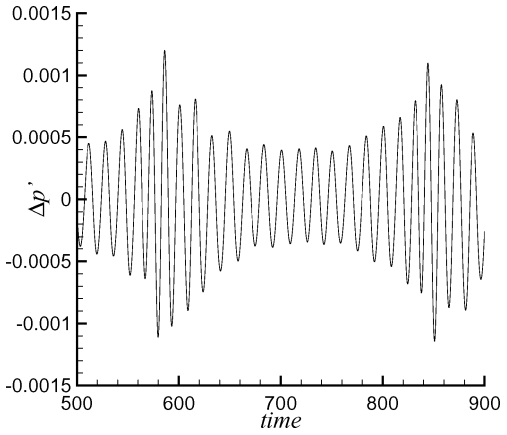

c) PEE

Fig. 6 Time history of instantaneous pressure fluctuation $\Delta p'$ at $r = 60D$ and $\theta = 90$ deg.

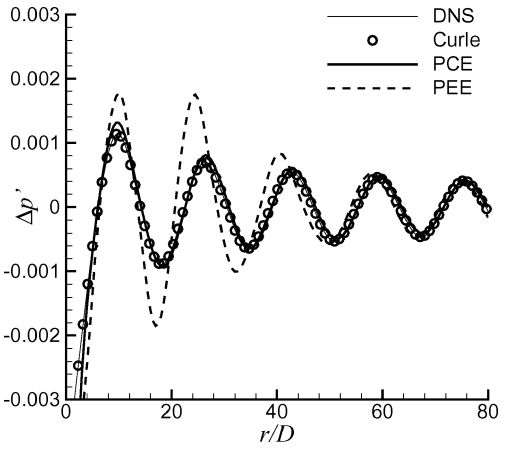

a) Instantaneous pressure fluctuation $\Delta p'$ variation along the $\theta = 90$ deg line

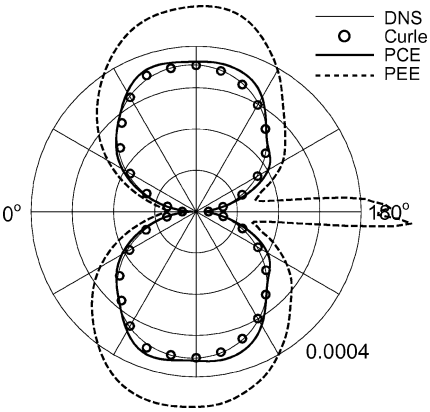

b) Directivity of pressure fluctuation (rms) $\Delta p'_{\mathrm{rms}}$ at $r = 60D$

Fig. 7 Comparison of pressure fluctuation $\Delta p'$.

spurious perturbed vorticity fields around the cylinder, as well as in the downstream wake, shown in Fig. 8a. Notice that the perturbed vorticity field predicted by PEE already appears to be close to the incompressible vorticity field around the cylinder. The PCE result, however, shows that there is no significantly generated ω' field near the cylinder by $(\boldsymbol{u}' \cdot \nabla)\Omega$.

In Fig. 9, the reconstructed compressible vorticity fields ($\omega = \Omega + \omega'$) calculated by PCE and PEE are compared with that of DNS. The compressible vorticity field predicted by PCE appears almost identical to the DNS solution, but the PEE solution shows the compressible vorticity field considerably modified by false generation of ω' near the cylinder. This is due to the unphysical production of ω' and the lack of its diffusion. The present comparison indicates that 1) the coupling effect between the incompressible vorticity and the perturbed velocities must be treated carefully in the hydrodynamic/acoustic splitting method and 2) the near-field dynamics of perturbed vorticity is correctly handled by the present PCE.

Figure 10 also shows the instantaneous compressible flowfields of density, pressure, and temperature reconstructed by the perturbed solutions of PCE with the incompressible flow solution. The near-field compressible flowfields are found to be quite close when compared with the DNS solution. Figure 10 indicates that the density and temperature fields are also well captured by the present new perturbed energy equation. This remarkable achievement of PCE is due to the inclusion of perturbed viscous stresses and the new perturbed energy equation, both of which greatly contribute to improve the near-field compressibility effects.

B. Computational Efficiency of PCE

The main advantage of the hydrodynamic/acoustic splitting method is that one can use different grids for hydrodynamic and acoustic calculations. Because an acoustic length scale is much larger than the hydrodynamic at low Mach number, use of a fine hydrodynamic grid with a rather coarse acoustic grid is preferred so that a proper selection of minimal grid size for the acoustic grid allows the hydrodynamic and acoustic calculations to have the same time step. The DNS calculation may suffer from the time step being severely restricted by a Courant–Friedrichs–Lewy (CFL) condition.

In this study, the hydrodynamic calculation was performed with the DNS grid (201×201), whereas the PCE is solved on a coarse acoustic grid (121×151) with a minimal normal spacing of $\Delta r_{\min,A} (= \Delta r_{\min,H} / M_\infty)$ (Fig. 11). This allows the hydrodynamic and acoustic calculations to share the same time step and, consequently, speeds up the acoustic calculation of the present test problem at $M_\infty = 0.3$. Here, the subscript A denotes acoustic and H denotes hydrodynamic. For PCE calculation, a linear interpolation method[16] based on a conservation principle is also used to transfer the incompressible flow variables from the fine hydrodynamic grid

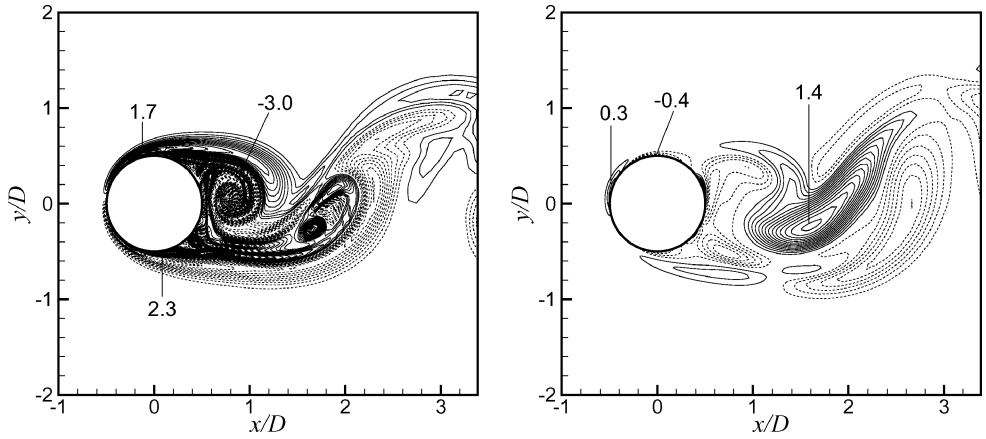

a) ω' contours

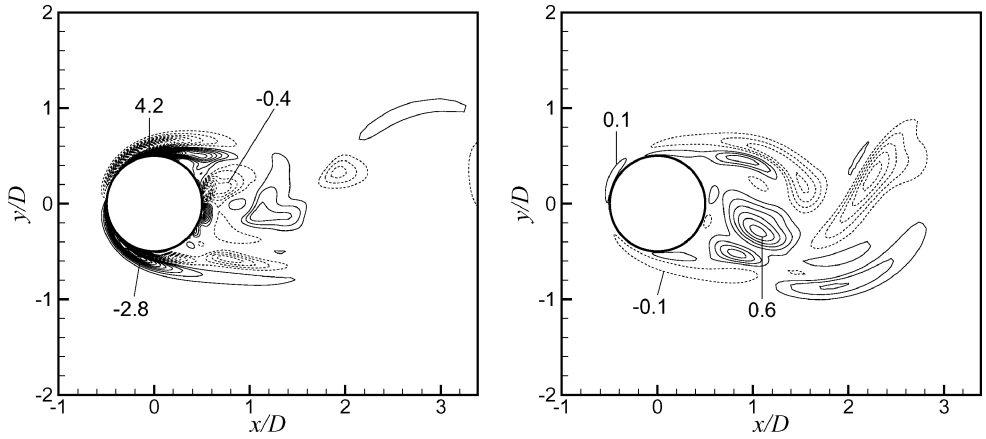

b) $(\boldsymbol{u}' \cdot \nabla)\Omega$ contours

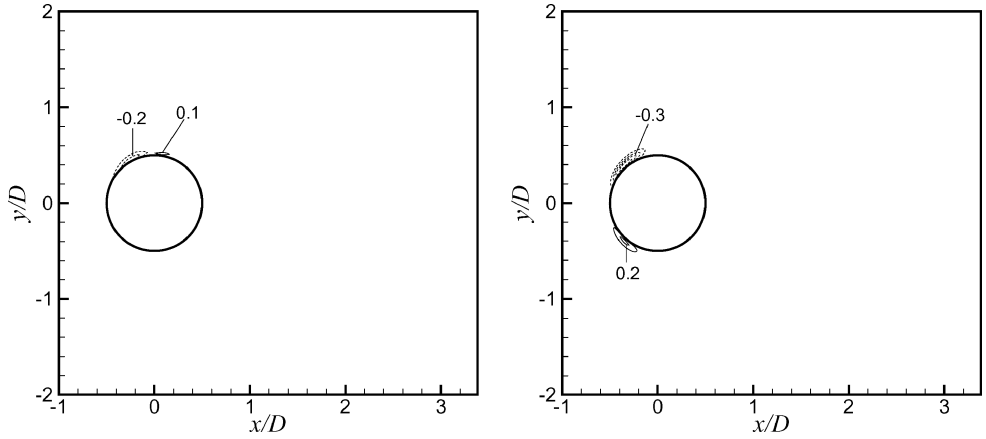

c) $\Omega(\nabla \cdot \boldsymbol{u}')$ contours

Fig. 8 Contours of instantaneous perturbed vorticity and its source terms (contour level difference, 0.1): left, PEE and right, PCE.

to the coarse acoustic grid. The computational results of PCE with the coarse acoustic grid are presented in Figs. 12–14. Figure 12 shows that the instantaneous pressure fluctuation contours are very close compared with the DNS solution, except that some small high-frequency fluctuations are observed in the near field. This is caused by a rapid diffusion of vortices in the wake region due to the grid coarseness. The amplitudes and wave length of pressure flucutation along the $\theta = 90$ deg line are also in excellent agreement with the DNS solution, and the perturbed vorticity field around the cylinder is well resolved on the coarse acoustic grid, as shown in Figs. 13 and 14.

The computational efficiency of the present PCE is now shown by estimating the computation time required for each method: DNS, incompressible Navier–Stokes (INS), and PCE with fine and coarse grids. For example, total computation time T required for obtaining an acoustic field from a time-periodic flow may be expressed as

$$T = T_D + T_P = (\alpha + 1)Nt_P \tag{21}$$

where T_D and T_P are, respectively, the computation time required for the development of a periodic stage and for a whole span of periodic stage of one's interest and α is a ratio between T_D and T_P, which is a problem-dependent constant. Also, t_P is the computation time for one period of flow unsteadiness, and N is a number of periods in T_P.

If t_I is the computation time per iteration and n is the number of iterations per period (based on a time step for INS), then the computation time for one period required by INS is written as

$$t_{P,\mathrm{INS}} = nt_{I,\mathrm{INS}} \tag{22}$$

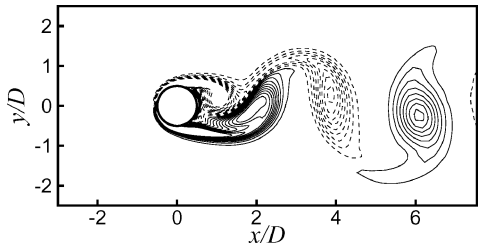

a) DNS (ω)

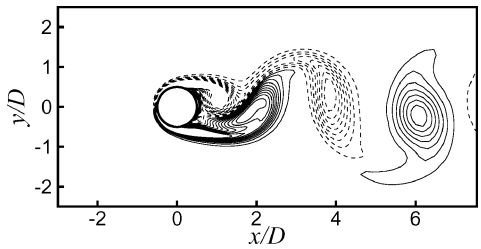

b) PCE ($\omega = \Omega + \omega'$)

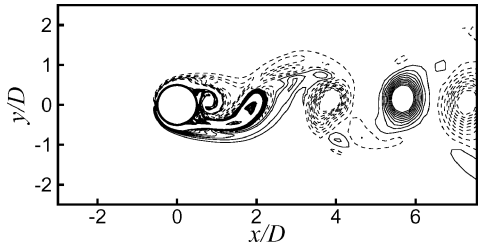

c) PEE ($\omega = \Omega + \omega'$)

Fig. 9 Contours of instantaneous compressible vorticity (20 contours between −1.0 and 1.0).

For DNS and PCE with the fine grid, however, the number of iterations for one period increases $1/M_\infty$ times, because the time step is restricted M_∞ times by the numerical stability condition. Hence,

$$t_{P,\mathrm{DNS}} = (n/M_\infty)t_{I,\mathrm{DNS}}, \qquad t_{P,\mathrm{PCE}(f)} = (n/M_\infty)t_{I,\mathrm{PCE}(f)} \tag{23}$$

For PCE with coarse grid, if one enlarges the minimal grid spacing $1/M_\infty$ times so that the time step of PCE can be comparable with that of INS, then

$$t_{P,\mathrm{PCE}(c)} = nt_{I,\mathrm{PCE}(c)} \tag{24}$$

The total computation time required for DNS and PCE for fine and coarse grids can be written as

$$T_{\mathrm{DNS}} = (\alpha + 1)N(n/M_\infty)t_{I,\mathrm{DNS}}$$

$$T_{\mathrm{PCE}(f)} = \alpha Nnt_{I,\mathrm{INS}} + N(n/M_\infty)\left(t_{I,\mathrm{INS}} + t_{I,\mathrm{PCE}(f)}\right)$$

$$T_{\mathrm{PCE}(c)} = \alpha Nnt_{I,\mathrm{INS}} + Nn\left(t_{I,\mathrm{INS}} + t_{I,\mathrm{PCE}(c)}\right) \tag{25}$$

Now, a speed-up factor of PCE is defined for fine grid as

$$\Psi_{\mathrm{PCE}(f)} = \frac{T_{\mathrm{DNS}}}{T_{\mathrm{PCE}(f)}} = \frac{(\alpha + 1)t_{I,\mathrm{DNS}}}{(\alpha M_\infty + 1)t_{I,\mathrm{INS}} + t_{I,\mathrm{PCE}(f)}} \tag{26}$$

and for coarse grid as

$$\Psi_{\mathrm{PCE}(c)} = \frac{T_{\mathrm{DNS}}}{T_{\mathrm{PCE}(c)}} = \frac{1}{M_\infty}\frac{(\alpha + 1)t_{I,\mathrm{DNS}}}{(\alpha + 1)t_{I,\mathrm{INS}} + t_{I,\mathrm{PCE}(c)}} \tag{27}$$

Figure 15 shows speed-up factors for PCE with fine and coarse acoustic grids, using $t_{I,\mathrm{DNS}}$, $t_{I,\mathrm{INS}}$, $t_{I,\mathrm{PCE}(f)}$, and $t_{I,\mathrm{PCE}(c)}$ listed in Table 1 for the present cylinder tone problem. Notice that the PCE with fine grid is only efficient for large α, regardless of M_∞, whereas the PCE with coarse grid tends to be more efficient as

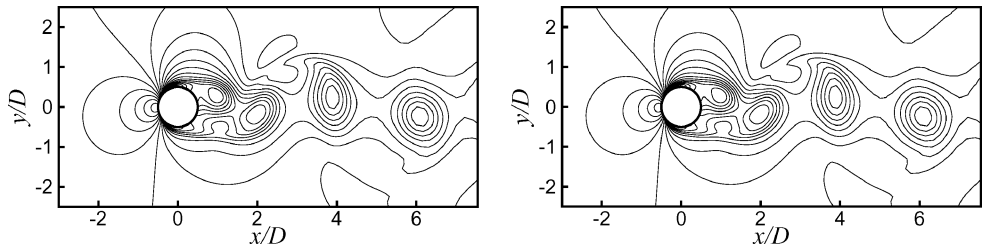

a) Density

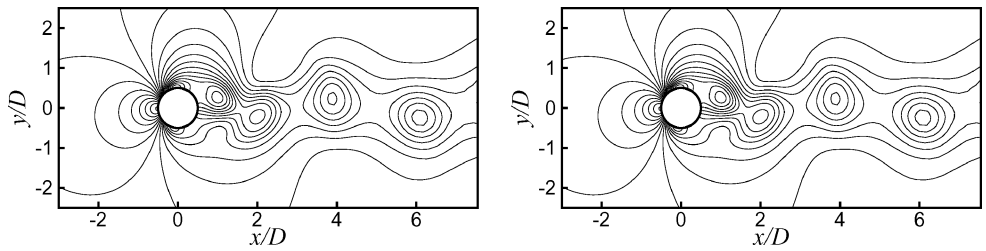

b) Pressure

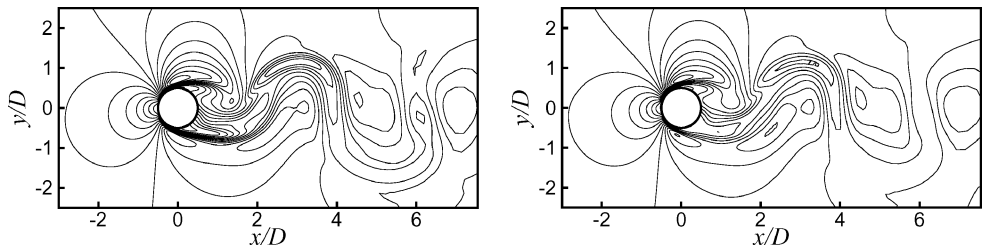

c) Temperature

Fig. 10 Comparison of instantaneous compressible near fields [PCE, reconstructed from $p = P + p'$, $\rho = \rho_0 + \rho'$, and $T = \gamma(P + p')/(\rho_0 + \rho')$]: left, DNS and right, PCE.

Table 1 CPU time for each method[a]

Method	CPU time per iteration, s	Time step corresponding to CFL = 0.5 (nondimensionalized by D/U_∞)[b]	CPU time for one period of vortex shedding ($5D/U_\infty$), s	CPU time for development of periodic vortex shedding, s
DNS (201×201)	0.424	1.5×10^{-3}	1413	14130
INS (201×201)	0.377	5×10^{-3}	377	3770
PCE (fine grid) (201×201)	0.597	1.5×10^{-3}	1992	——
PCE (coarse grid) (121×151)	0.217	5×10^{-3}	217	——

[a]Pentium 4 processor, 2.4 GHz. [b] $\mathrm{CFL} = U_\infty \Delta t/\Delta x$ for INS; $\mathrm{CFL} = U_\infty \Delta t/(M_\infty \Delta x)$ for DNS and PCE.

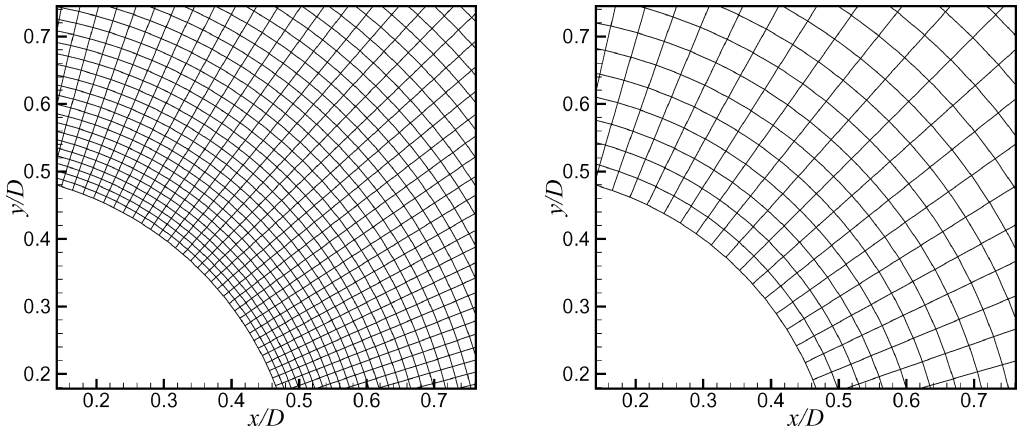

a) Hydrodynamic grid **b) Acoustic grid**

Fig. 11 Fine hydrodynamic and coarse acoustic grids.

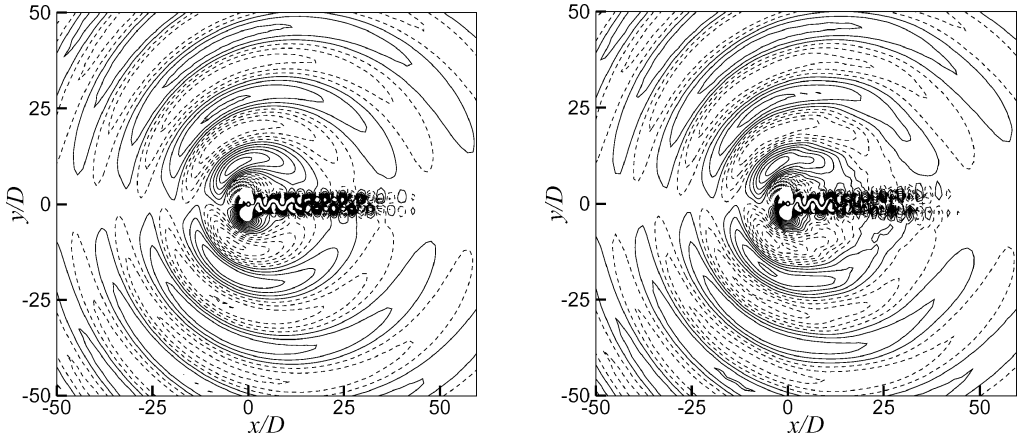

a) DNS **b) PCE (coarse acoustic grid)**

Fig. 12 Contours of instantaneous pressure fluctuation $\Delta p'$ around a circular cylinder ($M_\infty = 0.3$, $Re_D = 200$, 20 contours between -0.002 and 0.002).

M_∞ approaches zero, regardless of α. In fact, $\Psi_{\mathrm{PCE}(c)}$ is inversely proportional to M_∞, reaching infinity at the incompressibility limit. This is, however, only true if the minimal grid spacing is enlarged $1/M_\infty$ times. In practice, one must use a limiting factor $K_{\max}$ for enlargement of the minimal grid spacing. The speed-up factor of PCE for coarse grid can be modified as

$$\Psi_{\mathrm{PCE}(c),\mathrm{lim}} = \frac{(\alpha+1)t_{I,\mathrm{DNS}}}{(\alpha M_\infty + 1/k)t_{I,\mathrm{INS}} + (1/k)t_{I,\mathrm{PCE}(c)}} \tag{28}$$

where $k = \min(1/M_\infty, K_{\max})$. The modified speed-up factor is shown in Fig. 15 for $K_{\max} = 5$. In this case, the minimal grid spacing of the coarse acoustic grid is limited to be enlarged five times that of the fine hydrodynamic grid, that is, $\Delta r_{\min,A} = \Delta r_{\min,H}/M_\infty$ for $M_\infty > 0.2$ and $\Delta r_{\min,A} = 5\Delta r_{\min,H}$ for $M_\infty \le 0.2$. If this grid is used for PCE, then the speed-up factor is approximately in the range of 5–7 for $M_\infty < 0.2$ (with $\alpha = 1$). In the present test case ($M_\infty = 0.3$ and $\alpha = 1$), the computational efficiency of PCE was not achieved with fine grid, that is, $\Psi_{\mathrm{PCE}(f)} = 0.8$, whereas the PCE with coarse grid is approximately three times faster than the DNS, that is, $\Psi_{\mathrm{PCE}(c)} = 2.91$.

The computed results clearly illustrate that a consistent acoustic solution can be obtained by PCE with the coarse grid, exploiting the grid-splitting concept, which is considered a unique feature of the viscous/acoustic splitting method. It is also well demonstrated that significant computational efficiency can be achieved by PCE, and this efficiency will be greatly appreciated in three-dimensional turbulent flow noise prediction cases. A numerical study on the selection of optimal grid for acoustic calculation will be pursued further.

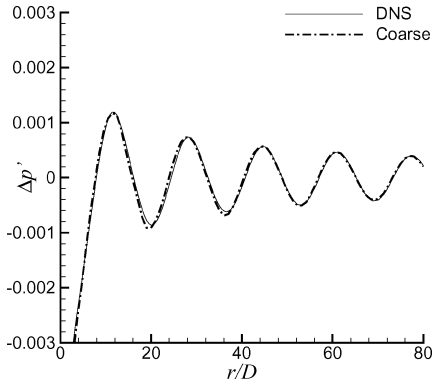

Fig. 13 Instantaneous pressure fluctuation $\Delta p'$ variation along the $\theta = 90$ deg line.

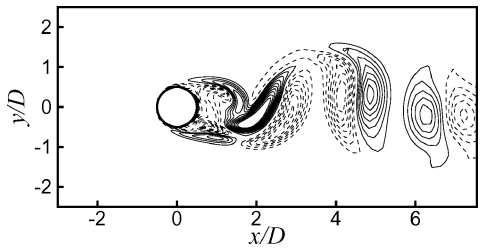

a) Fine acoustic grid

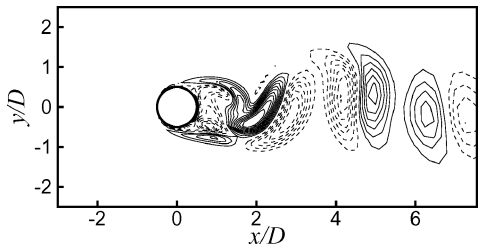

b) Coarse acoustic grid

Fig. 14 Contours of instantaneous perturbed vorticity (20 contours between −1.0 and 1.0).

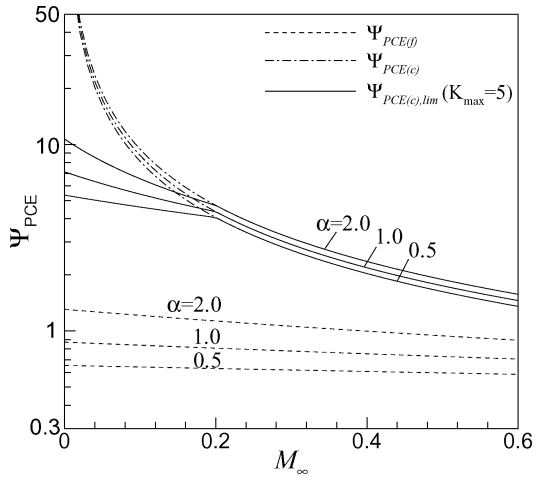

Fig. 15 Speed-up factor Ψ of PCE (*f*, fine acoustic grid; *c*, coarse acoustic grid; and lim, with limiter).

VI. Conclusions

In the present study, it is shown that for noise from a wall-bounded shear flow at low Mach number a coupling effect between the incompressible vorticity and the perturbed velocities can significantly be manifested near the wall through the convection of incompressible vorticity Ω by the perturbed velocity $\boldsymbol{u}'$. For this reason, the PEE used in previous splitting methods yield acoustic solutions significantly affected by false generation of perturbed vorticity near the wall through the coupling effect. It is also shown that this coupling effect is mainly caused by a production term $(\boldsymbol{u}' \cdot \nabla)\Omega$ in the perturbed vorticity transport equation.

To handle properly the near-field compressibility effect, a set of PCE is proposed. The PCE is validated for a dipole tone of laminar flow past a circular cylinder at $M_\infty = 0.3$ and $Re_D = 200$. The computational results show that not only the far-field acoustics but also the reconstructed compressible near fields are in excellent agreement with the DNS solution that was also validated by Curle's acoustic analogy solution at $r = 60D$. At the same time, a substantial amount of deviations are found in the PEE solution. This remarkable achievement of PCE is due to the perturbed viscous stresses included in the momentum equations and a new perturbed energy equation, both of which greatly contribute to improve the near-field compressibility effect.

Finally, the computational efficiency of the present PCE is demonstrated by employing an acoustic grid coarser than the hydrodynamic grid such that a time step can be shared for both. According to a speed-up factor of PCE derived by estimating the computation time required for DNS, INS, and PCE with fine and coarse grids, the PCE with coarse grid is approximately three times faster than the DNS for the present cylinder tone problem and the speed-up factor can be increased up to 5–7 for Mach number less than 0.2.

References

[1]Hardin, J. C., and Pope, D. S., "An Acoustic/Viscous Splitting Technique for Computational Aeroacoustics," *Theoretical Computational Fluid Dynamics*, Vol. 6, No. 5–6, 1994, pp. 323–340.

[2]Hardin, J. C., and Pope, D. S., "Sound Generation by Flow over a Two-Dimensional Cavity," *AIAA Journal*, Vol. 33, No. 3, 1995, pp. 407–412.

[3]Shen, W. Z., and Sorenson, J. N., "Comment on the Aeroacoustic Formulation of Hardin and Pope," *AIAA Journal*, Vol. 37, No. 1, 1999, pp. 141–143.

[4]Shen, W. Z., and Sorenson, J. N., "Aeroacoustics Modeling of Low-Speed Flow," *Theoretical Computational Fluid Dynamics*, Vol. 13, No. 4, 1999, pp. 271–289.

[5]Shen, W. Z., and Sorenson, J. N., "Aeroacoustic Modeling of Turbulent Airfoil Flows," *AIAA Journal*, Vol. 39, No. 6, 2001, pp. 1057–1064.

[6]Slimon, S. A., Soteriou, M. C., and Davis, D. W., "Computational Aeroacoustics Simulations Using the Expansion About Incompressible Flow Approach," *AIAA Journal*, Vol. 37, No. 4, 1999, pp. 409–416.

[7]Slimon, S. A., Soteriou, M. C., and Davis, D. W., "Development of Computational Aeroacoustics Equations for Subsonic Flows Using a Mach Number Expansion Approach," *Journal of Computational Physics*, Vol. 159, No. 2, 2000, pp. 377–406.

[8]Lee, D. J., and Koo, S. O., "Numerical Study of Sound Generation Due to a Spinning Vortex Pair," *AIAA Journal*, Vol. 33, No. 1, 1995, pp. 20–26.

[9]Lele, S. K., "Compact Finite Difference Schemes with Spectral-Like Resolution," *Journal of Computational Physics*, Vol. 103, No. 1, 1992, pp. 16–42.

[10]Inoue, O., and Hatakeyama, N., "Sound Generation by a Two-Dimensional Circular Cylinder in a Uniform Flow," *Journal of Fluid Mechanics*, Vol. 471, 2002, pp. 285–314.

[11]Visbal, M. R., and Gaitonde, D. V., "High-Order-Accurate Methods for Complex Unsteady Subsonic Flows," *AIAA Journal*, Vol. 37, No. 10, 1999, pp.1231–1239.

[12]Rizzetta, D. P., Visbal, M. R., and Gaitonde, V., "Large-Eddy Simulation of Supersonic Compression-Ramp Flow by High-Order Method," *AIAA Journal*, Vol. 39, No. 12, 2001, pp. 2283–2292.

[13]Gaitonde, D., Shang, J. S., and Young, J. L., "Practical Aspects of Higher-Order Numerical Schemes for Wave Propagation Phenomena," *International Journal for Numerical Methods in Engineering*, Vol. 45, No. 12, 1999, pp. 1849–1869.

[14]Freund, J. B., "Proposed Inflow/Outflow Boundary Condition for Direct Computation of Aerodynamic Sound," *AIAA Journal*, Vol. 35, No. 4, 1997, pp. 740, 741.

[15]Amsden, A. A., and Harlow, F. H., "A Simplified MAC Technique for Incompressible Fluid Flow Calculations," *Journal of Computational Physics*, Vol. 6, No. 2, 1970, pp. 322–325.

[16]Moon, Y. J., and Liou, M. S., "Conservative Treatment of Boundary Interface for Overlaid Grids and Multi-Level Grid Adaptations," *AIAA 9th Computational Fluid Dynamics Conference*, AIAA, Washington, DC, 1989, pp. 480–494.

K. Ghia
Associate Editor